University of Huddersfield

University of Huddersfield Repository

Claus, Daniel, Maiden, Andrew M., Zhang, Fucai, Sweeney, Francis, Humphry, Martin J., Schluesener, Hermann and Rodenburg, John M.

Quantitative phase contrast optimised cancerous cell differentiation via ptychography

Original Citation

Claus, Daniel, Maiden, Andrew M., Zhang, Fucai, Sweeney, Francis, Humphry, Martin J., Schluesener, Hermann and Rodenburg, John M. (2012) Quantitative phase contrast optimised cancerous cell differentiation via ptychography. Optics Express, 20 (9). p. 9911. ISSN 1094-4087

This version is available at http://eprints.hud.ac.uk/16052/

http://eprints.hud.ac.uk/

Quantitative phase contrast optimised cancerous cell differentiation via ptychography

Daniel Claus,[1,*] **Andrew M. Maiden,**[1] **Fucai Zhang,**[1]
Francis G. R. Sweeney,[1] **Martin J. Humphry,**[2] **Hermann Schluesener,**[3]
and John M. Rodenburg[1]

[1] *Kroto Research Institute, University of Sheffield,S3 7HQ, Sheffield, UK*
[2] *Phase Focus Ltd., S3 7HQ, Sheffield, UK*
[3] *Division of Immunopathology of the Nervous System, University of Tuebingen, D-72076
Tuebingen, Calwer Str. 3, Germany*

[*]d.claus@sheffield.ac.uk

Abstract: This paper shows that visible-light ptychography can be used to distinguish quantitatively between healthy and tumorous unstained cells. Advantages of ptychography in comparison to conventional phase-sensitive imaging techniques are highlighted. A novel procedure to automatically refocus ptychographic reconstructions is also presented, which improves quantitative analysis.

References and links

1. W. Hoppe, "Diffraction in inhomogeneous primary wave fields: 1. principle of phase determination from electron diffraction interference," Acta Crystallogr. A **25**, 495–501 (1969).
2. J. M. Rodenburg, A. C. Hurst, A. G. Cullis, B. R. Dobson, F. Pfeiffer, O. Bunk, C. David, K. Jefimovs, and I. Johnson, "Hard x-ray lensless imaging of extended objects," Phys. Rev. Lett. 98, 034801 (2007).
3. P. Thibault, M. Dierolf, A. Menzel, O. Bunk, C. David, and F. Pfeiffer, "High-resolution scanning x-ray diffraction microscopy," Science **321**, 379–382 (2008).
4. M. Dierolf, A. Menzel, P. Thibault, P. Schneider, C. M. Kewish, R. Wepf, O. Bunk, and F. Pfeiffer, "Ptychographic x-ray computed tomography at the nanoscale," Nature **46**, 436–439 (2010).
5. A. M. Maiden, M. J. Humphry, F. Zhang, and J. M. Rodenburg, "Superresolution imaging via ptychography," J. Opt. Soc. Am. A **28**, 604–612 (2011).
6. M.Guizar-Sicairos and J. R. Fienup, "Phase retrieval with transverse translation diversity:a nonlinear optimization approach," Opt. Express **16**, 7264–7278 (2008).
7. P. Thibault, M. Dierolf, O. Bunk, A. Menzel, and F. Pfeiffer, "Probe retrieval in ptychographic coherent diffractive imaging," Ultramicroscopy **109**, 338–343 (2009).
8. A. M. Maiden and J. M. Rodenburg, "An improved ptychographical phase retrieval algorithm for diffractive imaging," Ultramicroscopy **109**, 1256–1262 (2009).
9. G. Popescu, *Quantitative Phase Imaging of Cells and Tissues,* 1st ed. (McGraw-Hill, 2011).
10. K. A. Nugent, "Coherent methods in the X-ray sciences," Adv. Phys. **59**, 1–99 (2010).
11. H. J. Schluesener and T. Xianglin, "Selection of recombinant phages binding to pathological endothelial and tumor cells of rat glioblastoma by in-vivo display," J. Neurol. Sci. **224**, 77-82 (2004).
12. Sciencelearn.org, "What is cancer," http://www.sciencelearn.org.nz/Contexts/See-through-Body/Looking-closer/What-is-cancer.
13. J. W. Goodman, *Introduction to Fourier Optics,* 2nd ed. (McGraw-Hill, 1996).
14. C. P. McElhinney, B. M. Hennely, and T. J. Naughton, "Extended focused imaging for digital holograms of macroscopic three-dimensional objects," Appl. Opt. **47**, D71–D78 (2008).

15. D. Claus, "High resolution digital holographic synthetic aperture applied to deformation measurement and extended depth of field method," Appl. Opt. **49**, 3187–3198 (2010).
16. H. Haferkorn, *Optik, Physikalisch-technische Grunlagen und Anwendungen* (Willey-VCH, 2003).
17. S. L. Shorte and F. Frischknecht, editors, *Imaging cellular and molecular biological functions* (Springer, 2007).
18. P. Rabinovitch, "Introduction to cell cycle analysis," http://www.phnxflow.com/Introduction to Cell Cycle Analysis.pdf.
19. Z. Hameed and C. Wang, "Edge detection using histogram equalization and multi-filtering process," in *Proceedings of IEEE Conference on Circuits and Systems* (IEEE, 2011), pp. 1077–1080.
20. G. S. Benham, "Practical aspects of objective lens selection for confocal and multiphoton digital imaging techniques," in *Cell biological applications of confocal microscopy*, B. Matsumoto ed. (Academic Press, 2002), pp. 245–299.
21. L. Granero, V. Micó, Z. Zalevsky, and J. Garcia, "Synthetic aperture superresolved microscopy in digital lensless fourier holography by time and angular multiplexing of the object information," Appl. Opt. **49**, 3187–3198 (2010).
22. M. D. Iturbe Castillo, D. Sánchez de-la Llave, R. Ramos García, L. I. Olivos-Pérez, and M. Rodríguez-Ortiz L. A. González, "Real-time self-induced nonlinear optical zernike-type filter in a bacteriorhodopsin film," Opt. Eng. **40**, 2367–2368 (2003).

1. Introduction

We present a novel method for the quantitative differentiation of unstained tumorous and healthy cells via visible-light ptychography. The accuracy of the technique is further enhanced by using an automated refocusing algorithm. The term 'ptychography' relates to a method first proposed by Hoppe [1] as a solution to the phase problem that arises in X-ray and electron crystallography. The word ptychography follows from the Greek words 'ptux' meaning to fold and 'graphein' meaning to write. The 'folding' term refers to the convolution theorem upon which ptychography is based. The similarity of the name to holography was presumably intentionally chosen, since ptychography, like holography, is a coherent diffraction imaging technique that results in the recovery of the complex object wave. Hence the many advantages known from digital holography are equally applicable to ptychography, such as lensless imaging and quantitative phase measurement. An advantage of ptychography over digital holography is the removal of the need for a reference beam. This results in increased environmental stability, a less complex setup (with regards to optical elements needed) and an intrinsic aberration free reconstruction. Due to these benefits ptychography has successfully been established as a lensless imaging technique in the X-ray community: see for example [2–4] and has shown some very useful properties in the visible regime such as intrinsic super-resolution capability, as described in [5].

In ptychography only diffraction patterns from the coherently illuminated object are recorded. Either the coherent illumination (which can be formed either by a simple aperture upstream or downstream of the object and/or by a lens) or the object is moved laterally to generate diffraction patterns at a series of known positions, which are recorded on a digital sensor. The illuminated areas of the object at each position overlap, which introduces a redundancy into the data. This redundancy is used to solve the phase ambiguity problem (i.e. to calculate the phase of the diffraction patterns which can only be measured in intensity). Although originally postulated at the end of the 1960s, only recently with the advent of iterative algorithms [6–8] has ptychography become computationally practical.

An inherent property of ptychography is that the phase of an image reconstructed from diffraction pattern intensity has very high contrast and is quantitatively accurate over an adjustable wide field-of-view. This is particularly useful to investigate biological samples, which are generally transparent and so do not show high amplitude contrast in a conventional optical microscope. It is therefore not easy to visualise such cells unless a staining process is applied (see Figs. 1(a) and 1(b), white light microscopy with and without staining, respectively), which may harm or even kill the cell. For translucent samples, the scattered light (which contains all

the structural information about the object) is 90° out of phase with the unscattered beam (see the Rayleigh-Sommerfeld diffraction integral in Eq. (1), indicated by the factor $\frac{1}{i}$).

$$u(x',y') \propto \frac{1}{i\lambda} \int\limits_{-\infty}^{\infty} \int\limits_{-\infty}^{\infty} u(x,y) \frac{\exp(ikr)}{r} \cos\varepsilon \, dA \qquad (1)$$

where $u(x',y')$ is the complex light distribution in the diffraction plane and $u(x,y)$ is the complex light distribution in the object plane, ε is the diffraction angle and r is the radius defined by the wavefront curvature with respect to its intersection point in the diffraction plane. When the object is weak (first Born approximation), this means that the modulus of the image (hence its intensity) is negligibly affected by the scattered waves. Conventional Zernike phase contrast microscopy partly resolves this problem by reducing the amplitude of the undiffracted light and by introducing an additional 90° phase shift into the diffracted light. In the image, both terms (scattered and unscattered) now interfere strongly (they are in phase or anti-phase with one another), greatly increasing the visibility of the specimen. However, conventional Zernike phase contrast microscopy is not quantitative and suffers from artifacts, such as 'halos' which surround the edges of phase structures in the specimen. Ptychography and other quantitative phase imaging techniques, as discussed in [9] and [10], result in a true phase map of the object. Ptychography unlike these other techniques results in the recovery of the complex illumination function and the complex object transmission function. Hence, the recovered complex object transmission function does not hold any artifacts caused by the object illuminating beam. Furthermore, due to the application of a curved illumination, an object point is scanned by different incident plane waves when moving the illumination function across the object. This results in speckle de-correlation by which the quality (signal to noise ratio) of the reconstructed image is improved.

This makes ptychography an ideal tool for the investigation of cells, the study of their motility and cell cycles. In the results presented here, unstained cells are examined. Figure 1(c) and Fig. 1(d) show the same field of view imaged by both Zernike phase contrast microscopy and by ptychography. Zernike phase contrast microscopy can lead to a false impression of the phase, as shown on the submarine-shaped structure in Figs. 1(c) and 1(d). The true quantitative ptychographic phase map exhibits very low phase retardation for the encircled structure (Fig. 1(d)), whereas the Zernike phase contrast image displays high values at this location (Fig. 1(c)).
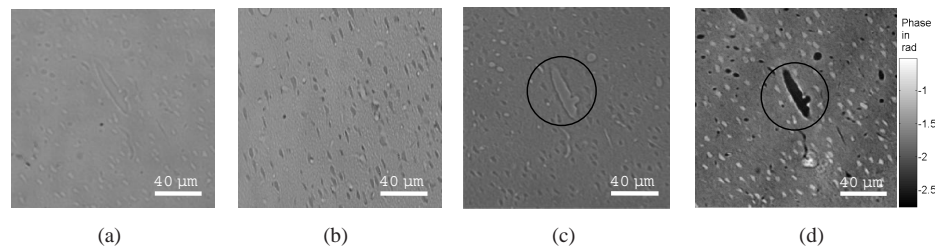

Fig. 1. Biological tissue visualisation via: (a) white light microscopy (unstained), (b) white light microscopy combined with cell staining (dye used hemalum), (c) Zernike phase contrast microscopy (unstained), (d) ptychography (unstained).

2. Experimental setup

The setup can be configured in a lensless or lens-based setup; the latter was chosen for this experiment (see Fig. 2). The lens based setup enables imaging of the object, hence ensuring
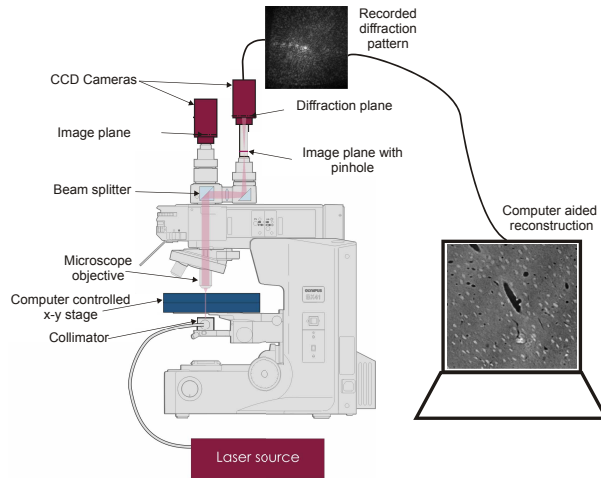
Fig. 2. Ptychographic microscopy using a lens-system.

that only the area of interest is investigated. A 10x microscope objective with a NA of 0.25 in combination with a laser diode emitting at 675 nm was used. The ptychographic process is performed by positioning a pinhole in the image plane, which serves as an aperture stop. The diffraction patterns are recorded at a distance of 95 mm from the image plane. The object is laterally displaced to a series of overlapping adjacent positions (typically 70 % overlap) via an x-y positioning stage. In this manner the large data redundancy required in order to overcome the phase ambiguity problem is generated. This configuration was chosen to minimise the effect of empty magnification. Empty magnification occurs if the smallest resolvable object detail δ is displayed by more than one pixel $\Delta x''$. The maximum resolution obtained is defined by the wavelength λ and numerical aperture NA of the microscope objective employed, such that

$$\delta = 0.5 \frac{\lambda}{\text{NA}}. \tag{2}$$

The distance between the sensor (diffraction plane) and the image plane, as shown in Fig. 2, was chosen to ensure that the smallest resolvable object detail in the image plane (δM) can still be recovered:

$$d \leq \frac{\delta M N \Delta x'}{\lambda} \tag{3}$$

where M is the magnification of the microscope objective, N is the pixel number and $\Delta x'$ is the pixel size. The maximum distance between sensor and image is 151 mm (N=1024, Δ x'=7.4 μm). The pixel size in the reconstruction plane on the other hand can be calculated as:

$$\Delta x'' = \frac{\lambda d}{N \Delta x' M} \tag{4}$$

Using this configuration the ratio between smallest resolvable object detail $\delta = 1.35 \ \mu m$ [Eq. (2)] and the pixel-size $\Delta x'' = 0.85 \ \mu m$ [Eq. (4)] in the reconstructed ptychographic image was best with respect to the efficient usage of pixels, reducing the effect of empty magnification. A second camera was added to the system enabling the object to be surveyed and a region of interest selected in real time, as shown in Fig. 2.

Ptychographic reconstructions were performed using the so-called ePIE iterative algorithm described in [8]. This uses the recorded diffraction patterns to form an exit wave in the object

plane in both modulus and phase. It also exploits further redundancy in the data to recover the illumination function - or in this case, the exact form of the aperture in the image plane - thus requiring no detailed knowledge of the microscope optics. In the images presented here, 15x15 (225) diffraction patterns were processed, the object was laterally displaced between each recording position. The ptychographic data was recorded within 45 seconds. The algorithm was executed using 32 bit Matlab on a Intel Core 2 Quad CPU in combination with CUDA algorithm on the graphics processing unit (GPU). The two dimensional fast fourier transform and fourier shift functions were transferred to the GPU of type Nvidia GeForce GTX285 in order to speed up the processing time. The calculation terminated after 147 seconds.

3. Label free cell discrimination

The experimental setup was used for the investigation of transparent unstained biological cells. Healthy and tumorous rat brain cells were analysed and compared. The classical rat model C6 glioma was used. Briefly, rat C6 glioma cells were implanted into rat brains as described in [11]. Rats were killed and perfused by 4% paraformaldehyde solution and tissue embedded in paraffin. The procedure is identical to that used for the processing of human brain tumors. Sections of two micrometers thickness were taken from the trimmed wax blocks, mounted on microscope slides, dewaxed by Xylol and rehydrated. Sections were embedded and sealed by a coverslip.

In the ptychographic reconstruction tumorous and healthy cells could be distinguished by their structure (Fig. 3): tumorous cells have irregular nuclei, are more dense and differ in size and shape whereas healthy cells are more sparsely distributed and more regular in size and shape, as discussed in [12]. The visual discrimination is furthermore supported by statistical parameters such as variance and by the histogram of the reconstructed phase. Although in this case structural differences are clear, we show below that statistical properties of the ptychographic phase images can also be used to automatically and reliably identify healthy and tumorous cells. Both the visual discrimination and discrimination via statistical parameters is best undertaken if the reconstruction is in very accurate focus, as comparatively demonstrated in Figs. 3(a), 3(b) and Fig. 4(a).

However, like conventional images, ptychographic reconstructions are rarely in perfect focus, due to inaccuracies in measurements of the experimental parameters (the wavelength, camera-object distance and amount of shift between adjacent probe positions). Fortunately, because the images generated by ptychography are quantitative in amplitude and phase, they can be refocussed after acquisition of the data. Refocusing (via the angular spectrum method [13]) was automated using the variance as a guidance, since an in-focus image is obtained when the variance in the phase data is highest, as discussed in [14, 15]. After resizing the obtained phase image to half its size to reduce the calculation time, a window of 10x10 pixels, within
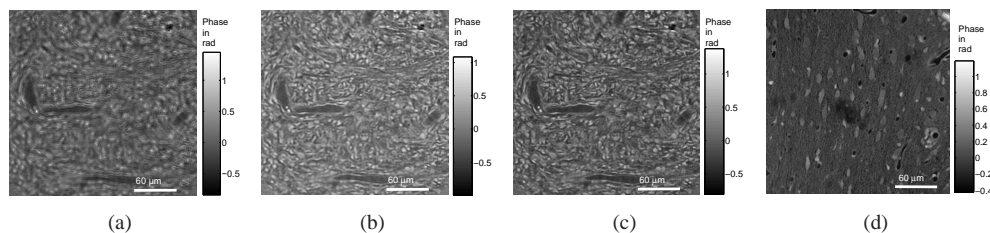

Fig. 3. Phase reconstructed data: (a) tumorous unfocused, (b) tumorous refocused by 18.5 μm, (c) tumorous refocused by 13.2 μm, (d) healthy refocused.
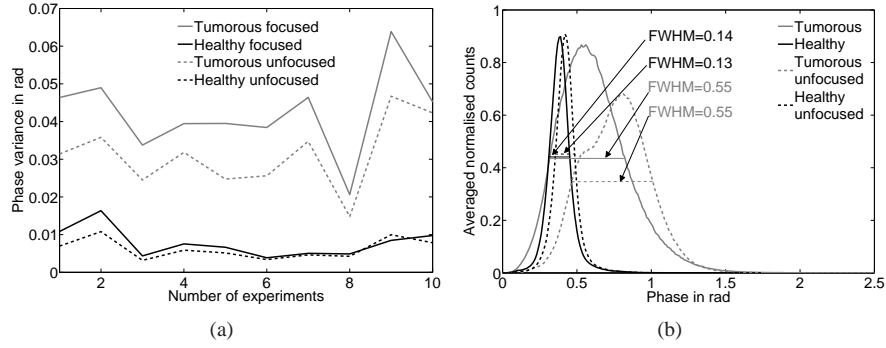
Fig. 4. Analysed phase reconstructed data: (a) variance plot, (b) histogram plot.

which the variance was calculated, was scanned across the image. The variance values were then summed up to obtain a single value representing this particular axial imaging position. The same procedure was then applied to a number of other calculated axial imaging positions separated by half the depth of field (DOF) (adapted from [16]).

$$DOF = \frac{\Delta x''}{NA} + \frac{\lambda}{NA^2}. \tag{5}$$

The DOF obtained is 14.2 μm. The method described above is accurate but computationally intensive. To reduce this computation time, it was decided to apply a curve fitting procedure to the calculated variance values, which required an investigation of the behaviour of the sharpness (S) with respect to defocus. The sharpness of an image is ill-defined: no precise description exists in the literature. We used the modulation transfer function (MTF) to define the sharpness. The sharpness is then described by the sum of the product of the MTF value and spatial frequency, ν. In other words it represents the MTF weighted spatial frequency response the optical system possesses, such that

$$S(\nu) = \int [MTF(\nu) \cdot \nu] \, d\nu. \tag{6}$$

Without loss of generality, let us treat the pinhole truncated image obtained from the microscope objective as a new object. The MTF corresponds to the modulus of the auto-correlation function of the exit pupil as discussed in [13]. The exit pupil is defined as the image of the aperture stop. In the case where there is no aperture stop other than the lens aperture, then the exit pupil and the aperture stop coincide. In our case, the optical imaging via a lens is replaced by a numerical (synthetic) lens, which is in an iterative manner applied to the recorded diffraction pattern. The lateral dimensions of the numerical lens match with the sensor size (whereas the focal length of the numerical lens is half the camera object distance). Hence, the lateral sensor dimensions define the exit pupil dimensions. The defocus is accounted for in the exit pupil by the multiplication with a complex parabolic phase term, which results in the following phase distribution across the exit pupil:

$$\varphi(x', y') = kW(x', y') = -8\pi \frac{W_{max}(x', y')}{\lambda} \frac{x'^2 + y'^2}{D^2} \tag{7}$$

where x' and y' are the lateral coordinates in the exit pupil (diffraction plane), k is the wave number $\left(k = \frac{2\pi}{\lambda}\right)$, D is the diameter of the exit pupil, W is the phase of the introduced wave aberration, and W_{max} represents the maximum phase aberration. The normalised sum of the product of MTF and spatial frequency response has then been plotted against different defoci,

represented by the ratio of maximum defocus wave aberration error over the wavelength employed ($\frac{W_{max}}{\lambda}$). The result shown in Fig. 5(a) suggests that the sharpness can be approximated by a Gaussian curve. The goodness of this fit was evaluated by a squared correlation coefficient ($R^2 = 0.97$), which confirms the validity of the Gaussian fit. The ripples in Fig. 5(a) occur at those positions when the optical transfer function (OTF, MTF=|OTF|) goes from positive to negative values and vice versa.

The obtained in focus position via Gaussian fitting (18.5 μm) has then been compared with the calculated variance values while applying a smaller refocusing step size (1/10 of the DOF resulting in an in-focus position at 13.2 μm). The result of this analysis is graphically represented in Fig. 5(b). The variance curve with finer refocusing step width exhibits a skewness, which may have been caused by aberration errors from the microscope objective.

The difference (5.3 μm) between the in-focus position obtained via Gaussian fitting and calculated variance value is within the DOF (14.2 μm) and is therefore acceptable. This can be confirmed by the quality of the numerical reconstructions obtained at the corresponding positions, displayed in Fig. 3(b) (18.5 μm) and Fig. 3(c) (13.2 μm). Having corrected their focus via the proposed optimisation algorithm, statistical analysis was applied to the ptychographic images. The variance of the phase images was calculated for healthy and tumorous cells. In order to conduct a representative analysis ten experimental data sets of each healthy and tumorous unstained rat brain tissue have been investigated. The results of which are graphically represented in Fig. 4(a). From this, two statements can be drawn. Firstly, a tumorous brain cell possesses a larger phase variance than a healthy one. Secondly, the phase variance and the difference in phase variance (goodness of discrimination) between tumorous and healthy cells increases for the refocused image, resulting in improved reliability of the data.

Another indicator commonly used for imaging of biological cells is the histogram, as discussed in [17]. The histogram can be used to distinguish between different cell populations or different cell cycles [18], to determine the cell size and shape [19] or to adjust exposure parameters in order to record a high contrast image [20]. In our case the averaged histogram from ten experimental data sets for each healthy and tumorous cells has been calculated and plotted in Fig. 4(b), which shows that the histogram of a tumorous brain cell possesses an increased full width at half maximum (FWHM). In combination with the ptychographically obtained high contrast phase image, this analysis suggests that both the histogram and the variance value of quantitative phase images could be used to support cell discrimination in cancer research.
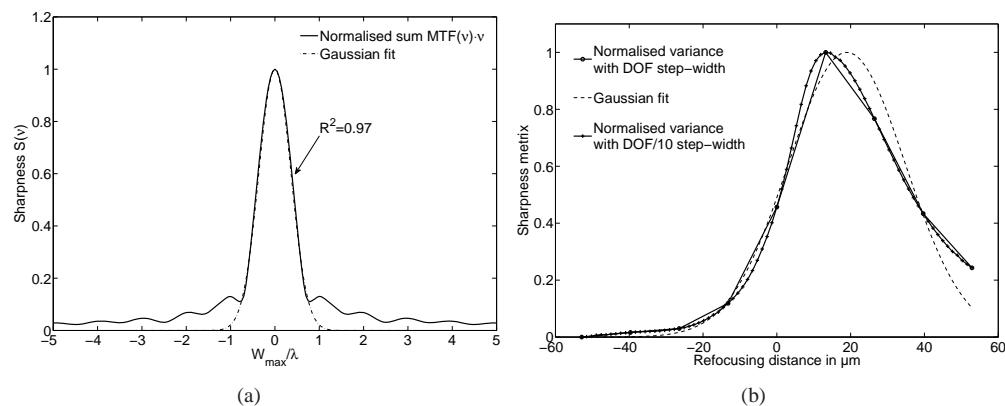

Fig. 5. (a) Graph: Sharpness (product MTF and v) vs de-focus, (b) Graph: Validation of Gaussian fitting procedure.

4. Conclusion and future work

The work discussed in this paper demonstrates improved phase contrast via ptychography, by which healthy and tumorous *unstained* rat brain cells could be discriminated. Ptychography enables a non-invasive and non-destructive full-field investigation. We have shown that statistical parameters can be extracted from ptychographic phase images which can quantitatively complement cell discrimination. The ptychographic recording process introduces a large degree of speckle de-correlation, which results in an increased optical resolution and reduced speckle noise in the reconstructed image (similar to the synthetic aperture technique in digital holography as discussed in [15, 21]). The high quality of the ptychographic reconstruction and the high phase contrast suggest that the technique should be very valuable in a wide range of biomedical applications. Therefore future work will be focused on the application of ptychography for the investigation of human cells, cell cycles, discrimination of different cell populations and the monitoring of dynamic events. The imaging of transparent objects of very low phase modulation via phase contrast enhancement methods such as the implementation of a non-linear phase contrast method (as discussed in [22]) is another goal of future research. Moreover, the lens-based setup will be replaced by a lensless setup, which offers a larger degree of freedom without having to sacrifice optical resolution (see [5]).